



Review

Preparation of a $\text{Gd}_{0.1}\text{Ce}_{0.9}\text{O}_{2-\delta}$ interlayer for intermediate-temperature solid oxide fuel cells by spray coating

Dongfang Wang, Jianxin Wang, Changrong He, Youkun Tao, Cheng Xu, Wei Guo Wang*

Division of Fuel Cell and Energy Technology, Ningbo Institution of Materials Technology & Engineering, Chinese Academy of Sciences, 519 Zhuangshi Road, Ningbo 315201, PR China

ARTICLE INFO

Article history:

Received 15 April 2010

Received in revised form 29 May 2010

Accepted 2 June 2010

Available online 11 June 2010

Keywords:

Interlayer

Solid oxide fuel cell

Spray coating

ABSTRACT

Spray coating is widely used in industrial applications for the preparation of large, uniform thin films on various substrates due to its simplicity and cost-efficiency. To prevent reactions between a yttria-stabilised zirconia (YSZ) electrolyte and a $\text{La}_{0.6}\text{Sr}_{0.4}\text{Co}_{0.2}\text{Fe}_{0.8}\text{O}_{3-\delta}$ (LSCF) cathode, a $\text{Gd}_{0.1}\text{Ce}_{0.9}\text{O}_{2-\delta}$ (CGO) interlayer with a thickness of 2–3 μm is prepared on a YSZ electrolyte by spray coating. The results indicate that the properties of the CGO interlayer depend on its preparation conditions, including the powder pre-sintering temperature, the concentration of the dispersant and the sintering temperature. A densely packed CGO interlayer is obtained from a well-dispersed suspension of CGO powder pre-sintered at 750 °C with 6 wt.% PVP as a dispersant. After sintering at 1250 °C and 1300 °C, the CGO interlayer achieves an area special resistance (ASR) of 0.1 Ωcm^2 at 800 °C and 0.4 Ωcm^2 at 700 °C. Moreover, LSCF cells with a CGO interlayer obtain an average maximum power density greater than 600 mWcm^{-2} at 750 °C. Obvious diffusion of Sr is not observed in the cells, indicating that the CGO interlayer prepared by spray coating effectively blocks Sr diffusion.

© 2010 Elsevier B.V. All rights reserved.

Contents

1. Introduction	118
2. Experimental	120
2.1. Preparation of the CGO interlayer	120
2.2. Symmetric sample fabrication	120
2.3. Preparation and testing of LSCF–CGO cathode single cells	121
3. Results and discussion	121
3.1. Effect of PVP content and CGO pre-sintering temperature	121
3.2. The effect of sintering temperature on the CGO interlayer	121
4. Conclusion	123
Acknowledgements	123
References	123

1. Introduction

Solid oxide fuel cells (SOFC) are an environmental friendly energy technology that has drawn extensive attention over the last few decades [1]. To reduce the operating temperature of planar solid oxide fuel cells to temperatures between 600 °C and 850 °C, anode-supported fuel cell has been employed to decrease the thickness of the yttria-stabilised zirconia (YSZ) electrolyte [2]. In addition, Sr doped LaCoO_3 and LaFeO_3 perovskite oxides have been used as cathodic materials to improve the

power density at intermediate temperatures [3–6]. However, reactions between the YSZ electrolyte and the cathode materials result in the formation of $\text{La}_2\text{Zr}_2\text{O}_7$ and SrZrO_3 at the interface between the electrolyte and the cathode. The poor conductivity of $\text{La}_2\text{Zr}_2\text{O}_7$ and SrZrO_3 dramatically decreases the performance of the cell [7,8]. To prevent these reactions from occurring, a dense CGO (Gd doped ceria) interlayer is often introduced into the cell because CGO is compatible with cobaltite perovskite oxide and YSZ [7–10] cathodes. A proper method of film formation is essential to achieve a dense CGO interlayer. Vacuum deposition methods and wet ceramic methods are often employed to prepare dense CGO interlayers, including magnetron sputtering [11], electron beam physical vapour deposition [10], chemical vapour deposition (CVD), electrochemical vapour deposition (EVD),

* Corresponding author. Tel.: +86 574 87911363; fax: +86 574 87910728.
E-mail address: wgwang@nimte.ac.cn (W.G. Wang).

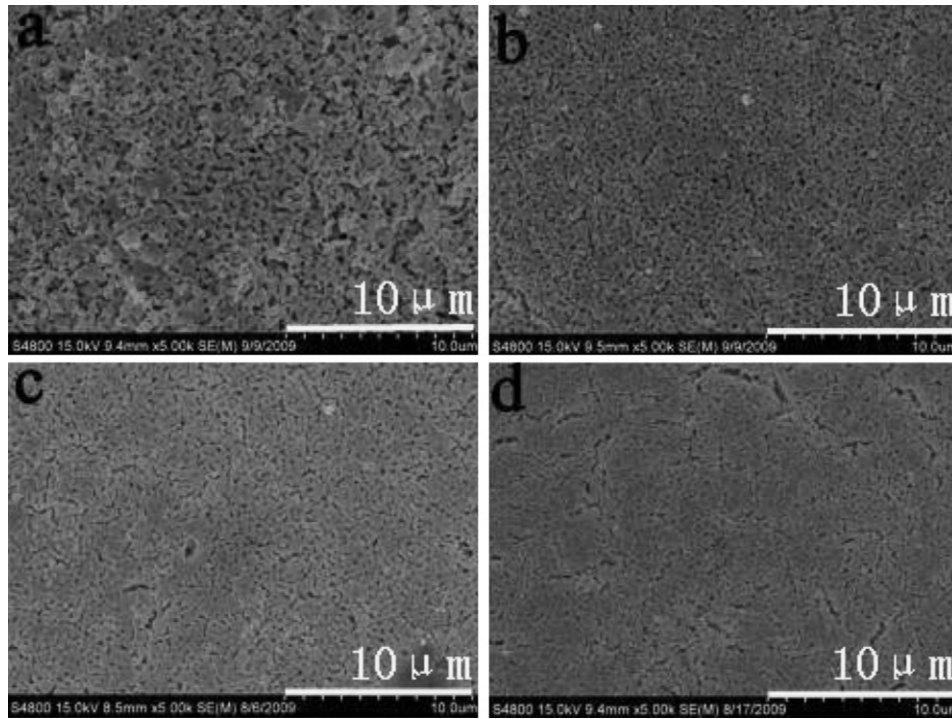


Fig. 1. SEM images of the surface of CGO interlayers, obtained by spraying a suspension with different concentrations of PVP: (a) 4 wt.%, (b) 5 wt.%, (c) 6 wt.% and (d) 8 wt.%.

atomic layer deposition (ALD), tape casting [12], sol–gel, screen printing and slurry coating [7,8,13]. Vacuum deposition methods can produce dense CGO interlayers at lower temperatures than wet ceramic methods but are more expensive and less efficient. A proper post-heat treatment process is also essential to achieving a dense CGO interlayer. The density of the CGO interlayer increases as the sintering temperature increases; however, reactions between YSZ and CGO become significant at tempera-

tures greater than 1200 °C, producing intermediate phases of (Zr, Ce)O₂-based solutions, which are poor ionic conductors. On the other hand, it is difficult to achieve a dense CGO interlayer with good interfacial contact at temperatures below 1300 °C [14,15]. Therefore, selecting an appropriate sintering temperature is essential.

In this study, green CGO interlayers were prepared by spray coating, which is a simple and cost-efficient method for the prepa-

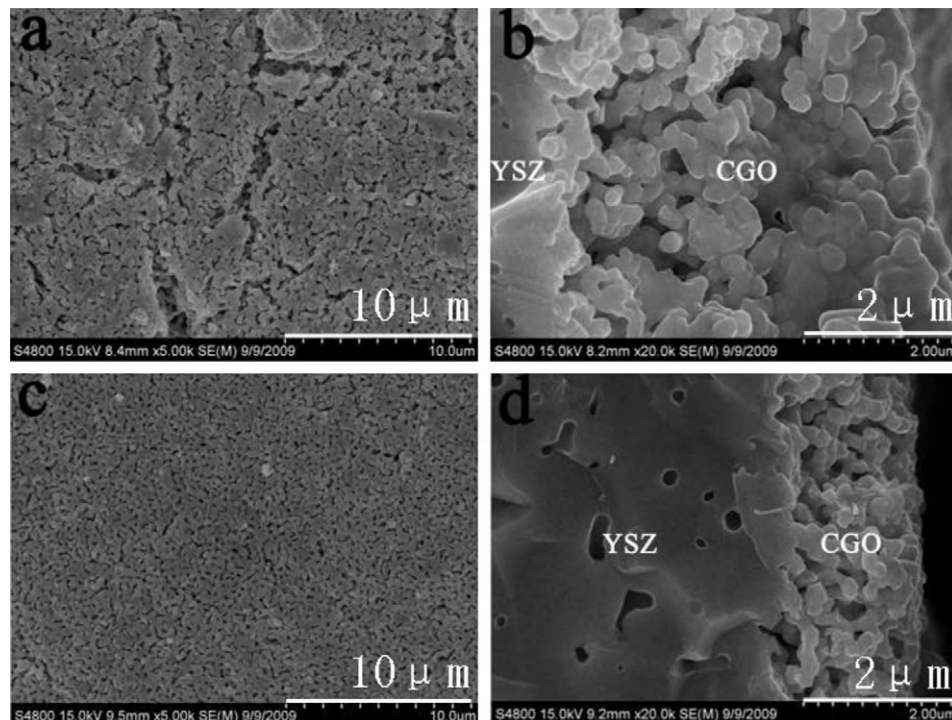


Fig. 2. SEM micrographs of the surface of CGO interlayers, prepared by pre-sintering CGO powder at: (a) and (b) 600 °C, (c) and (d) 750 °C.

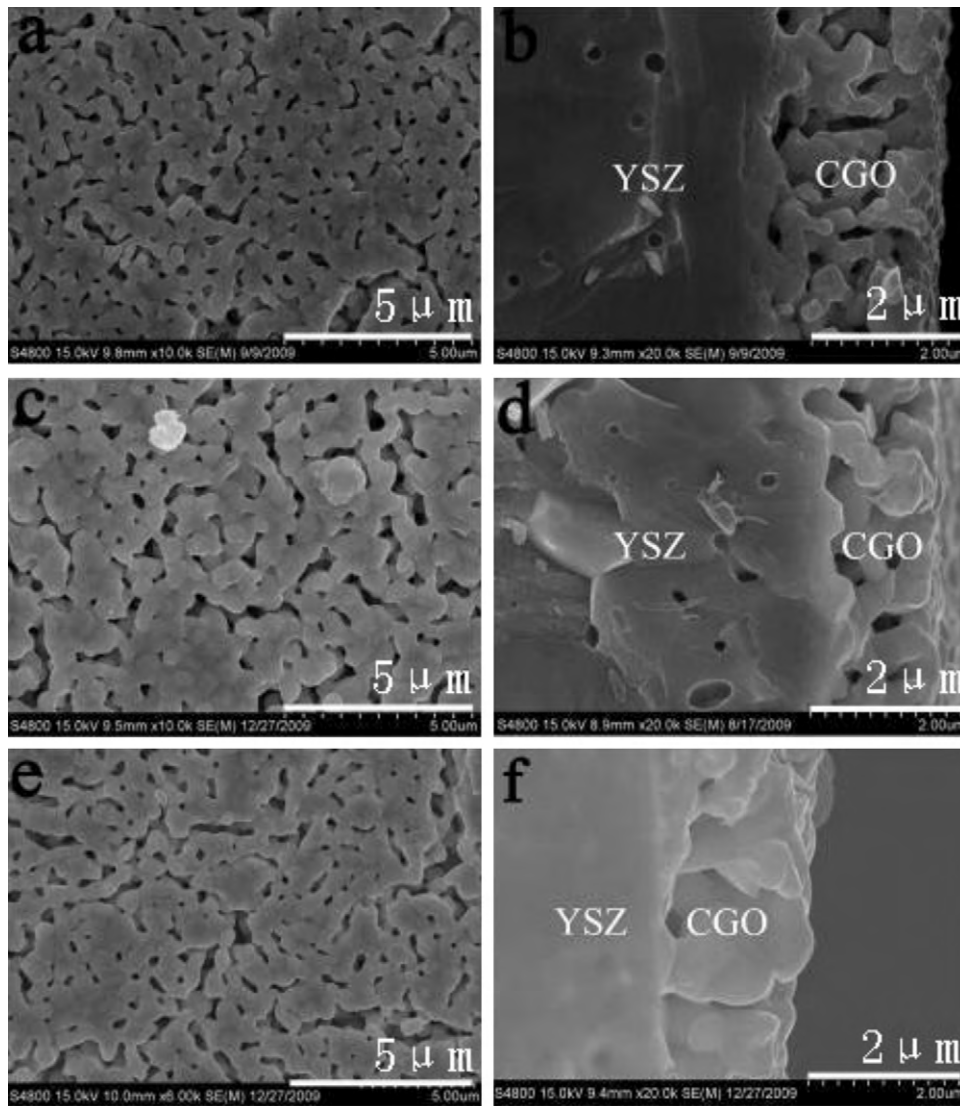


Fig. 3. SEM micrographs of the surface and cross-section of: (a) and (b) IS₁₂₀₀, (c) and (d) IS₁₂₅₀, (e) and (f) IS₁₃₀₀.

ration of large, uniform thin films on various substrates, and is suitable for many industrial applications. The sintering properties of the CGO interlayer were investigated by performing isothermal sintering between 1200 °C and 1300 °C. To evaluate the effect of spray coating on single cells, the CGO interlayer was fabricated on anode-supported cells with a LSCF (La_{0.6}Sr_{0.4}Co_{0.2}Fe_{0.8}O_{3-δ}) composite cathode.

2. Experimental

2.1. Preparation of the CGO interlayer

Gd_{0.1}Ce_{0.9}O_{2-δ} powder used to fabricate the CGO interlayer was prepared by the sol-gel method [16]. The average primary particle size of Gd_{0.1}Ce_{0.9}O_{2-δ} powder was approximately 44 nm. To determine the surface area of the powder, nitrogen adsorption-desorption experiments were conducted at 77 K, and a value of 18.8 m² g⁻¹ was obtained. The Ni-YSZ/YSZ substrate was produced by spraying a Ni-YSZ active layer and a YSZ electrolyte layer on a Ni-YSZ supported anode prepared by tape casting, followed by co-sintering at 1350 °C for 6 h. The surface and cross-section morphology of the substrates were investigated by field emission scanning electron microscopy (SEM) (S-4800, Hitachi).

CGO powder was calcined at 600 °C or 750 °C for 5 h. A suspension of the CGO powder was obtained by planetary ball milling pre-sintered CGO powder in ethanol for 48 h. To obtain a homogenous suspension, PVP was added as a dispersant, and the content of PVP was varied from 4 wt.% to 8 wt.%. A green CGO interlayer with a thickness of 2–3 μm was prepared by spraying the suspension on a YSZ electrolyte

with an air spray gun. Subsequently, the electrolyte was dried in air, and a CGO interlayer was obtained.

Samples of the green CGO interlayer were sintered at 1200 °C, 1250 °C and 1300 °C for 6 h and were labelled as IS₁₂₀₀, IS₁₂₅₀ and IS₁₃₀₀, respectively. The microstructure of the CGO interlayer was investigated with field emission scanning electron microscopy (SEM) (S-4800, Hitachi). Interfacial reactions between YSZ and CGO were identified by SEM and X-ray diffraction (XRD). X-ray diffraction analyses were performed on the CGO interlayer with a diffractometer (D8 Advance, Bruker) and Cu Kα radiation.

2.2. Symmetric sample fabrication

Symmetric samples with configurations of IS₁₂₀₀/YSZ/IS₁₂₀₀, IS₁₂₅₀/YSZ/IS₁₂₅₀ and IS₁₃₀₀/YSZ/IS₁₃₀₀ were prepared to evaluate the electrical properties of CGO interlayers sintered at different temperatures. The samples were obtained by spraying a suspension of CGO powder on both surface of 200-μm slices of YSZ, followed by isothermal sintering at 1200 °C, 1250 °C and 1300 °C, respectively. Platinum paste was brushed onto both surface of the symmetric samples, and the samples were heated at 950 °C for 2 h. Upon completion, the samples were cut into 7.1 mm by 7.1 mm blocks for impedance measurements. Complex impedance measurements were conducted with a frequency response analyser (Soltron 1260) at 500–900 °C in air, and the frequency was varied from 0.1 Hz to 1 MHz. The ohmic area special resistance (ASR) of the CGO interlayer was obtained from the following equation:

$$R = \frac{(R_1 - R_2)}{2}$$

where R , R_1 and R_2 are the ohmic area special resistances of the CGO interlayer, symmetric sample and YSZ slice, respectively. For comparison, the measurements were also conducted on the YSZ slice.

2.3. Preparation and testing of LSCF–CGO cathode single cells

Single cells with configurations of Ni–YSZ/YSZ/IS₁₂₀₀/LSCF–CGO, Ni–YSZ/YSZ/IS₁₂₅₀/LSCF–CGO and Ni–YSZ/YSZ/IS₁₃₀₀/LSCF–CGO were prepared by spraying a suspension of LSCF composite cathode materials on the CGO interlayer and sintering the electrode at 950 °C for 5 h [17]. Before the electrical properties were determined, the microstructure of the cells was evaluated by examining a cross-section of the single cells with a field emission scanning electron microscope (SEM) equipped with an energy dispersive X-ray analyser (EDS) (S-4800, Hitachi). Single cells with an active area of 4 cm × 4 cm were tested in a ceramic testing house. Pure hydrogen and air were used as the fuel and oxidant, respectively. Complex impedance measurements of the single cells were performed under open-circuit voltage (OCV) conditions with a frequency response analyser (Soltron 1260), and the frequency was varied from 0.1 Hz to 1 MHz at 850 °C.

3. Results and discussion

3.1. Effect of PVP content and CGO pre-sintering temperature

The formation of green CGO interlayers depends on the CGO suspension and the parameters of the spray coating process (i.e., flow velocity of the suspension, velocity of the motion system, distance between the nozzle and the substrate, etc.) [18]. In the present investigation, all of the parameters of the spray coating process were fixed; thus, the properties of the green CGO interlayer were determined by the CGO suspension, which was dominated by the concentration of dispersant. To optimise the dispersant concentration of the suspension, CGO interlayers were prepared with different amounts of PVP. Fig. 1 shows the SEM images of CGO interlayers prepared with different contents of PVP. As shown in the images, the number of cracks in the green body and the size of the micropores decreased as the content of PVP increased from 4 wt.% to 6 wt.%. Moreover, the results suggested that CGO particles were effectively dispersed in the suspension and adsorbed to the dispersant. However, as the content of PVP increased to 8 wt.%, the number of cracks in the interlayer also increased. Excess dispersant may cause bridging between particles, resulting in the formation of cracks. Thus, the results suggested that a well-dispersed suspension could be obtained with the addition of 6 wt.% PVP.

SEM micrographs of the surface and cross-section of the CGO interlayer prepared by pre-sintering CGO powder at different temperatures are shown in Fig. 2. After the sample was sintered at 1200 °C, the CGO powder agglomerated and cracks were observed at a pre-sintering temperature of 600 °C. The presence of cracks and agglomerates may be attributed to the high activity of the CGO powder. When the pre-sintering temperature was increased to 750 °C, the CGO interlayer was uniform and free of cracks. These results indicated that the optimal pre-sintering temperature of CGO powder was 750 °C.

3.2. The effect of sintering temperature on the CGO interlayer

SEM micrographs of IS₁₂₀₀, IS₁₂₅₀ and IS₁₃₀₀ are provided in Fig. 3, and the results revealed that a crack-free CGO interlayer was successfully obtained on the YSZ electrolyte. As shown in Fig. 4, SEM micrographs of the YSZ electrolyte indicated that the grain size of CGO increased from ca. 200 nm to 1 μm as the sintering temperature increased from 1200 °C to 1300 °C. Because the green CGO interlayer was prepared on a rigid YSZ electrolyte, CGO particles shrank during the sintering process, and pores in the CGO interlayer were observed after sintering. Moreover, the pores in the CGO interlayer became larger as the sintering temperature increased. SEM observation of the cross-section of the CGO interlayer revealed that the thickness of interlayer was ca. 2–3 μm. The

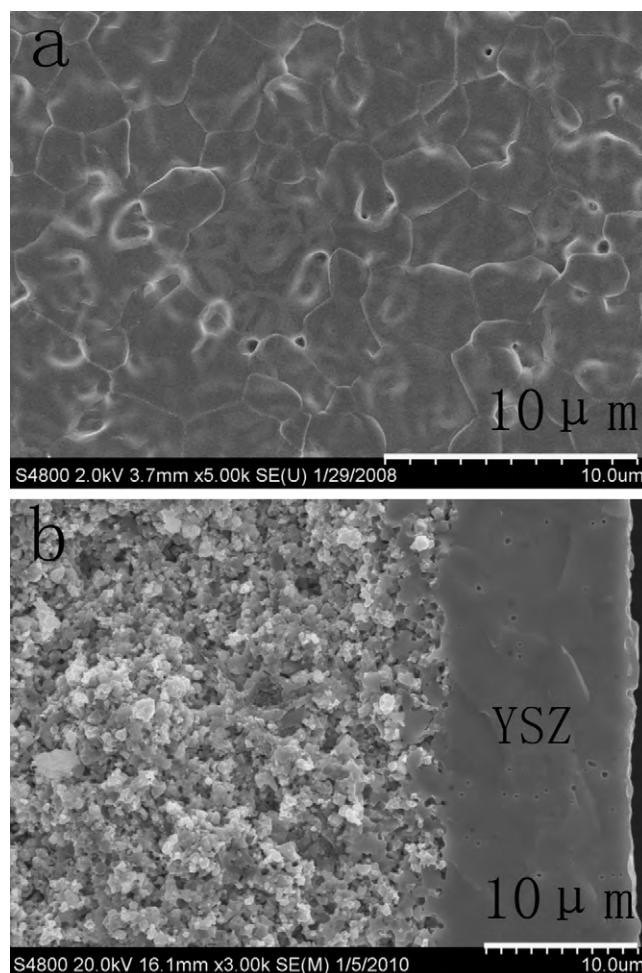


Fig. 4. SEM images of the surface and cross-section of the YSZ electrolyte.

results also suggested that the CGO interlayer was firmly attached to the YSZ electrolyte, and the contact between the interlayer and the electrolyte significantly improved as the sintering temperature increased.

XRD analyses were performed on the CGO interlayer of the samples, and the results are shown in Fig. 5. X-ray diffraction could not detect reactions between CGO and YSZ at a sintering temperature of 1200 °C. As the sintering temperature increased to 1250 °C and 1300 °C, evidence of the reactions became visible during X-ray diffraction analysis. As the sintering temperature increased, the peaks of CGO and YSZ shifted to higher angles and lower angles, respectively. Moreover, the shift in the peaks became larger as the sintering temperature of the sample increased. The (2 2 2) peak of CGO overlapped with the (3 1 1) peak of YSZ in the XRD spectra of IS₁₃₀₀ (Fig. 4b). The observed shift in the peak position was attributed to interdiffusion between YSZ and CGO, which increased with an increase in the sintering temperature of the sample. The observed results are in good agreement with those of previous studies [8,19,20].

The results of the symmetric samples tested in air at 500–900 °C are shown in Fig. 6, where the ASR of the CGO interlayer is plotted against the inverse of the testing temperature. The results indicated that the CGO interlayer possessed an ASR of ca. 0.1 Ω cm² at 800 °C and 0.4 Ω cm² at 700 °C, which was significantly less than the ASR of a CGO interlayer prepared by screen printing (ca. 0.4 Ω cm² at 800 °C and 1.6 Ω cm² at 700 °C [8]). However, the ASR of the CGO interlayer was much greater than the theoretical results of bulk CGO-10 (ca. 0.005 Ω cm² at 800 °C and 0.009 Ω cm² at 700 °C). The

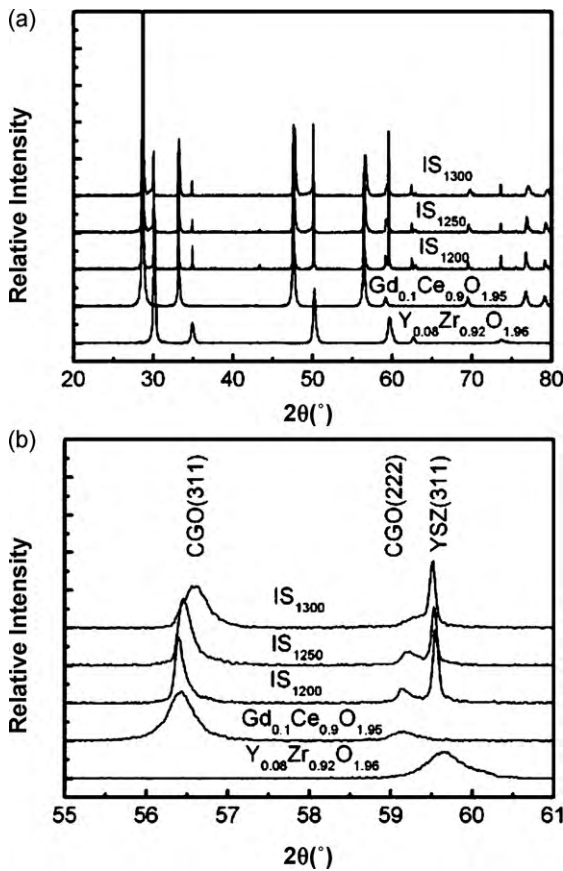


Fig. 5. XRD patterns of IS₁₂₀₀, IS₁₂₅₀ and IS₁₃₀₀.

ohmic area special resistance of the CGO interlayer consisted of the bulk resistance of the CGO interlayer (R_{bulk}) and the ohmic resistance of the YSZ/CGO interface ($R_{\text{interface}}$). R_{bulk} was influenced by the density of the CGO interlayer and the presence of defects, while $R_{\text{interface}}$ was affected by the contact between the YSZ electrolyte and CGO interlayer, as well as the reactions between them that occurred at the interface. Because the CGO interlayer was relatively thin, the ASR of the CGO interlayer was caused primarily by $R_{\text{interface}}$, resulting in an ASR that was much greater than the theoretical values. At temperatures below 700 °C, IS₁₂₀₀ possessed the lowest ASR, and the ASR of IS₁₃₀₀ was significantly less than those of IS₁₂₅₀ and IS₁₃₀₀ at temperatures greater than 700 °C. This result contradicts those of previous studies [8], which

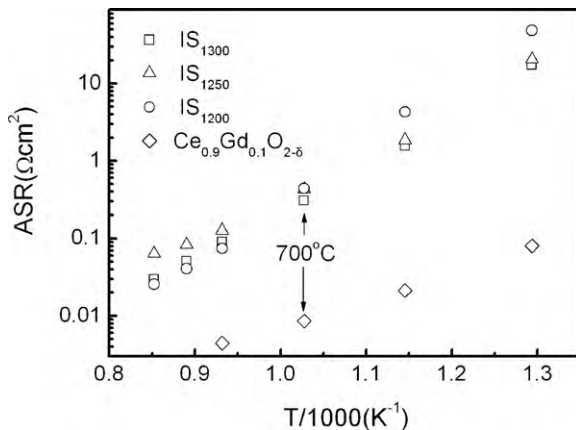


Fig. 6. Area specific resistance (ASR) plots of IS₁₂₀₀, IS₁₂₅₀, IS₁₃₀₀ and bulk CGO-10.

Table 1
The performance of the single cells.

Single cell	U_{ocv} (V) at 850 °C	R_s ($\Omega \text{ cm}^{-2}$) at 850 °C	P_{max} (mW/cm^2) at 750 °C
Ni-YSZ/YSZ/IS ₁₂₀₀ /LSCF-CGO	1.196	0.534	201
Ni-YSZ/YSZ/IS ₁₂₅₀ /LSCF-CGO	1.137	0.185	618
Ni-YSZ/YSZ/IS ₁₃₀₀ /LSCF-CGO	1.168	0.174	631

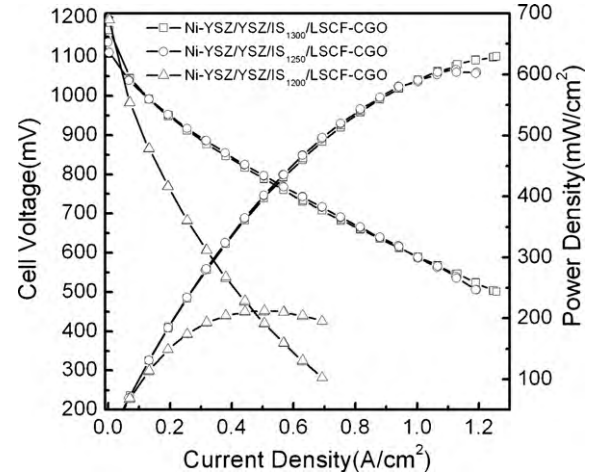


Fig. 7. I - V characteristics of the single cells at 750 °C.

suggested that a sintering temperature of 1200 °C resulted in the greatest conductivity. This disparity may be due to the densification process of the CGO interlayer and the simultaneous formation of (Zr,Ce)O₂-based solutions. As the sintering temperature increases, the CGO interlayer becomes denser and the interfacial contact between layers improves, which could lead to a reduction in the ASR. However, the results indicated that the amount of (Zr,Ce)O₂-based solutions at the YSZ/CGO interface increased with an increase in sintering temperature, causing the ASR of the cell to increase.

The results of impedance tests and the I - V characteristics of the single cells are provided in Table 1. Typical I - V characteristics of the single cells at 750 °C are shown in Fig. 7, where U_{ocv} , R_s and P_{max} denote the open-circuit voltage, ohmic resistance and maximum power density of the cells, respectively. The results in Table 1 indicated that the open-circuit voltage of the cells was greater than 1.1 V, which was in good agreement with the theoretical values. Cells consisting of Ni-YSZ/YSZ/IS₁₂₅₀/LSCF-CGO and Ni-YSZ/YSZ/IS₁₃₀₀/LSCF-CGO displayed a lower R_s and a higher P_{max} than a cell composed of Ni-YSZ/YSZ/IS₁₂₀₀/LSCF-CGO. The relatively high R_s and low P_{max} of the Ni-YSZ/YSZ/IS₁₂₀₀/LSCF-CGO cell suggested that a CGO interlayer sintered below 1200 °C could not effectively prevent reactions between YSZ and LSCF caused by Sr diffusion, and an increase in R_s and a deterioration in cell performance was observed. However, interlayers sintered at temperatures greater than 1250 °C could successfully prevent reactions between YSZ and LSCF. EDS analysis of the cross-section of Ni-YSZ/YSZ/IS₁₂₀₀/LSCF-CGO, Ni-YSZ/YSZ/IS₁₂₅₀/LSCF-CGO and Ni-YSZ/YSZ/IS₁₃₀₀/LSCF-CGO cells revealed that Sr, Ce, Gd, Zr, Y and La interdiffused between layers, and the results are shown in Fig. 8. The interdiffusion of Sr into the YSZ/CGO interface was detected in the cell composed of Ni-YSZ/YSZ/IS₁₂₀₀/LSCF-CGO; however, obvious Sr interdiffusion was not detected in Ni-YSZ/YSZ/IS₁₂₅₀/LSCF-CGO and Ni-YSZ/YSZ/IS₁₃₀₀/LSCF-CGO cells. These results are in good agreement with the aforementioned results and the overall performance of the cells. Moreover, obvious interdiffusion of Zr

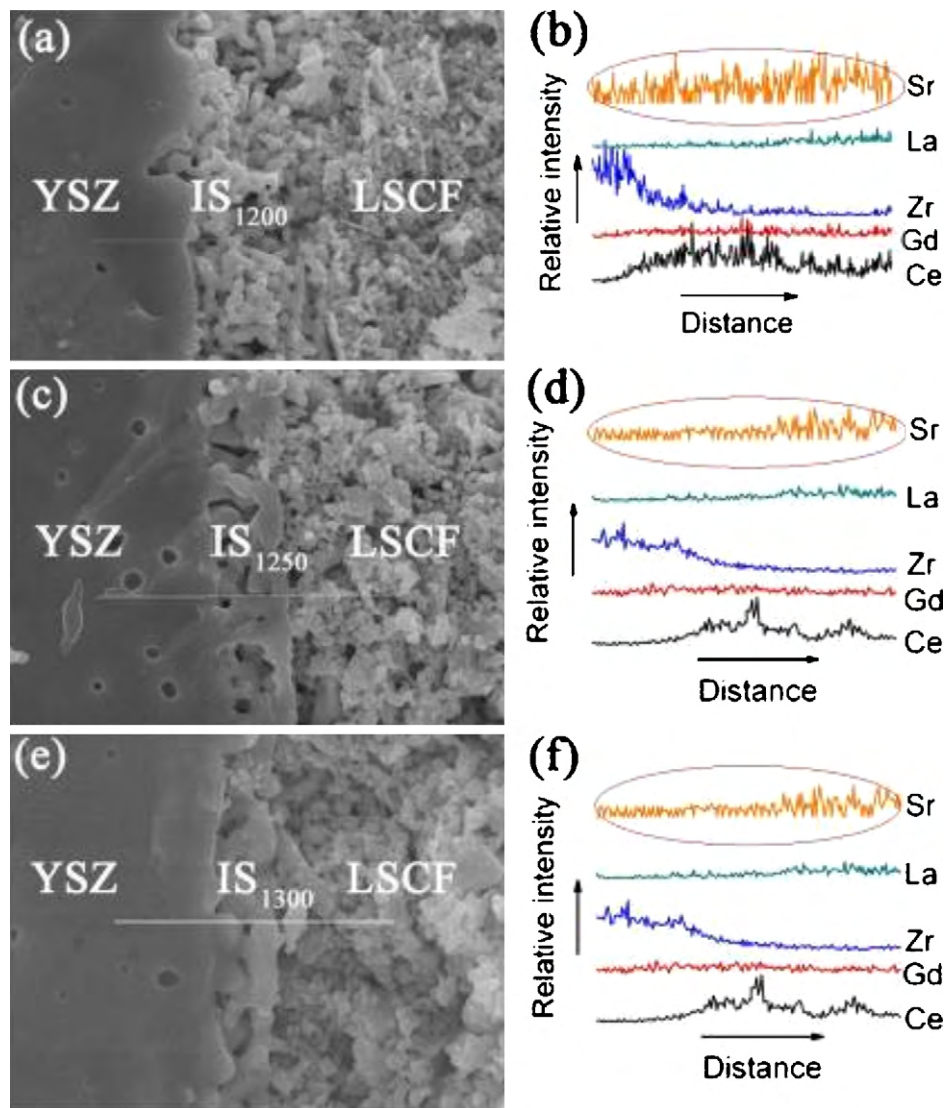


Fig. 8. EDS results of cells containing Ni-YSZ/YSZ/IS₁₂₀₀/LSCF-CGO (a and b), Ni-YSZ/YSZ/IS₁₂₅₀/LSCF-CGO (c and d) and Ni-YSZ/YSZ/IS₁₃₀₀/LSCF-CGO (e and f) before *I*-*V* characterisation.

and Ce was observed in all of the samples, which proved the formation of (Zr,Ce)₂O₃-based solutions at the YSZ/CGO interface.

4. Conclusion

A CGO interlayer was prepared by spray coating and isothermal sintering. The microstructure and electrical properties of the CGO interlayer were significantly dependent on the preparation conditions, including the powder pre-sintering temperature, the content of dispersant and the sintering temperature of the CGO interlayer. A dense CGO interlayer with a thickness of 2–3 μm was obtained from a suspension of CGO powder pre-sintered at 750 °C with 6 wt.% PVP. At a sintering temperature below 1300 °C, reactions between YSZ and CGO did not have a significant effect on the electrical properties of the material, and the ASR of the symmetric samples was ca. 0.1 Ω cm² at 800 °C and 0.4 Ω cm² at 700 °C. Thus, a CGO interlayer sintered at 1250 °C and 1300 °C effectively blocked Sr diffusion. Single cells with a CGO interlayer sintered at 1250 °C and 1300 °C exhibited a P_{\max} greater than 600 mW cm⁻² at 750 °C and an ohmic resistance less than 0.2 Ω cm² at 850 °C, indicating that the optimum sintering temperature of

the CGO interlayer prepared by spray coating was between 1250 °C and 1300 °C.

Acknowledgements

This work was supported in part by the National Natural Science Foundation of China (Grant No. 50902135), The Ningbo Municipal Natural Science Foundation of China (Grant No. 2009A610009) and the Chinese Academy of Sciences.

References

- [1] B. Stambouli, E. Traversa, *Renew. Sustain. Energy Rev.* 6 (2002) 433.
- [2] N.Q. Minh, *J. Am. Ceram. Soc.* 76 (1993) 563.
- [3] S.B. Adler, *Chem. Rev.* 104 (2004) 4791–4843.
- [4] R.M. Ormerod, *Chem. Soc. Rev.* 32 (2003) 17–28.
- [5] W.G. Wang, M. Mogensen, *Solid State Ionics* 176 (2005) 457–462.
- [6] F. Zhao, L. Zhang, Z. Jiang, C. Xia, F. Chen, *J. Alloys Compd.* 487 (2009) 781–785.
- [7] S.P. Simner, J.W. Stevenson, K.D. Meinhardt, N.L. Canfield, *The Electrochemical Society Proceedings Series*, 2001, p. 1051.
- [8] T.L. Nguyen, K. Kobayashi, T. Honda, Y. Iimura, K. Kato, A. Neghisi, K. Nozaki, F. Tappero, K. Sasaki, H. Shirahama, K. Ota, M. Dokiya, T. Tohru Kato, *Solid state Ionics* 175 (2004) 79–81.
- [9] S.P. Simner, J.P. Shelton, M.D. Anderson, J.W. Stevenson, *Solid State Ionics* 161 (2003) 11–18.

- [10] S. Uhlenbruck, N. Jordan, D. Sebold, H.P. Buchkremer, V.A.C. Haanappel, D. Stöver, *Thin Solid Films* 515 (2007) 4053–4060.
- [11] N. Jordan, W. Assenmacher, S. Uhlenbruck, V.A.C. Haanappel, H.P. Buchkremer, D. Stöver, W. Mader, *Solid State Ionics* 179 (2008) 919–923.
- [12] L.P. Meier, L. Urech, L.J. Gauckle, J. Eur. Ceram. Soc. 24 (2004) 3753–3758.
- [13] L. Lei Bi, S. Zhang, B. Lin, S. Fang, C. Xia, J. Alloys Compd. 473 (2009) 48–52.
- [14] X.-D. Zhou, B. Scarfino, H.U. Anderson, *Solid State Ionics* 175 (2004) 19–22.
- [15] A.A. Bukaemskiy, D. Barrier, G. Modolo, J. Alloys Compd. 472 (2009) 289–293.
- [16] T. Tao, J. Shao, J. Wang, W.G. Wang, J. Alloys Compd. 484 (2009) 729–733.
- [17] J. Shao, Y. Tao, J. Wang, C. Xu, W.C. Wang, J. Alloys Compd. 484 (2009) 263–267.
- [18] C. Ding, H. Lin, K. Sato, Y. Tsutai, H. Ohtaki, M. Iguchi, C. Wada, T. Hashida, J. Dispersion Sci. Technol. 30 (2009) 241–245.
- [19] N. Sakai, T. Hashimoto, T. Katsube, K. Yamaji, H. Negishi, T. Horita, H. Yokokawa, Y.P. Xiong, M. Nakagawa, Y. Takahashi, *Solid State Ionics* 143 (2001) 151.
- [20] H. Mitsuyasu, Y. Nonaka, K. Eguchi, *Solid State Ionics* 279 (1998) 113–115.